

Structures and Mechanical Properties of Natural and Synthetic Diamonds

Kazuhisa Miyoshi
Lewis Research Center, Cleveland, Ohio

The NASA STI Program Office . . . in Profile

Since its founding, NASA has been dedicated to the advancement of aeronautics and space science. The NASA Scientific and Technical Information (STI) Program Office plays a key part in helping NASA maintain this important role.

The NASA STI Program Office is operated by Langley Research Center, the Lead Center for NASA's scientific and technical information. The NASA STI Program Office provides access to the NASA STI Database, the largest collection of aeronautical and space science STI in the world. The Program Office is also NASA's institutional mechanism for disseminating the results of its research and development activities. These results are published by NASA in the NASA STI Report Series, which includes the following report types:

- **TECHNICAL PUBLICATION.** Reports of completed research or a major significant phase of research that present the results of NASA programs and include extensive data or theoretical analysis. Includes compilations of significant scientific and technical data and information deemed to be of continuing reference value. NASA's counterpart of peer-reviewed formal professional papers but has less stringent limitations on manuscript length and extent of graphic presentations.
- **TECHNICAL MEMORANDUM.** Scientific and technical findings that are preliminary or of specialized interest, e.g., quick release reports, working papers, and bibliographies that contain minimal annotation. Does not contain extensive analysis.
- **CONTRACTOR REPORT.** Scientific and technical findings by NASA-sponsored contractors and grantees.

- **CONFERENCE PUBLICATION.** Collected papers from scientific and technical conferences, symposia, seminars, or other meetings sponsored or cosponsored by NASA.
- **SPECIAL PUBLICATION.** Scientific, technical, or historical information from NASA programs, projects, and missions, often concerned with subjects having substantial public interest.
- **TECHNICAL TRANSLATION.** English-language translations of foreign scientific and technical material pertinent to NASA's mission.

Specialized services that complement the STI Program Office's diverse offerings include creating custom thesauri, building customized data bases, organizing and publishing research results . . . even providing videos.

For more information about the NASA STI Program Office, see the following:

- Access the NASA STI Program Home Page at **<http://www.sti.nasa.gov>**
- E-mail your question via the Internet to **help@sti.nasa.gov**
- Fax your question to the NASA Access Help Desk at (301) 621-0134
- Telephone the NASA Access Help Desk at (301) 621-0390
- Write to:
NASA Access Help Desk
NASA Center for Aerospace Information
7121 Standard Drive
Hanover, MD 21076



Structures and Mechanical Properties of Natural and Synthetic Diamonds

Kazuhisa Miyoshi
Lewis Research Center, Cleveland, Ohio

National Aeronautics and
Space Administration

Lewis Research Center

Available from

NASA Center for Aerospace Information
7121 Standard Drive
Hanover, MD 21076
Price Code: A03

National Technical Information Service
5287 Port Royal Road
Springfield, VA 22100
Price Code: A03

Chapter 8

Structures and Mechanical Properties of Natural and Synthetic Diamonds

8.1 Introduction and Historic Perspective

Diamond is an allotrope of carbon, joining graphite and the fullerenes as the major pure carbon structures. Diamond has a unique combination of properties: hardness, thermal conductivity, chemical and thermal inertness, and abrasion resistance. These properties make diamond attractive for a wide range of tribological applications, including solid lubrication. Presently, modern diamonds fall into four distinct categories: natural, high-pressure synthetic, chemical vapor deposited, and diamondlike carbon.

Natural diamond is produced at high pressures and temperatures in volcanic shafts. Rough natural diamonds (i.e., uncut and unpolished) were known and prized in antiquity [8.1]. They were first reported in India 2700 years ago. From India diamond trading moved gradually westward through Persia and the Roman Empire. However, the full beauty of diamond was not uncovered until faceting and polishing techniques were developed in the 14th and 15th centuries. Natural diamond is the primary source of diamond gemstones and by far the leader in terms of monetary value. However, in the last 100 years or so the scarcity and high cost of natural diamond have been challenged by the large-scale production of synthetic diamond.

The high-pressure synthesis essentially duplicates the natural high-pressure, high-temperature process [8.1, 8.2]. The French chemist A. L. Lavoisier found in 1772 that the product of diamond combustion was singular: carbon dioxide (CO_2). In 1814 the English chemist H. Davy proved conclusively that diamond was a crystalline form of carbon. He also showed that burning diamond produced only CO_2 , without the formation of aqueous vapor, indicating that it was free of hydrogen and water. Since that time many attempts have been made to synthesize diamond by trying to duplicate nature. These attempts, spread over a century, were unsuccessful. It was not until 1955 that the first unquestioned syntheses were achieved in the United States (General Electric), in Sweden (AESA), and in the Soviet Union (Institute for High-Pressure Physics). The advent of synthetic diamond and the rapid rise of industrial applications, particularly in wear, abrasive, and tool applications,

have drastically altered the industry. More changes, like the recent development of chemical-vapor-deposited diamond and diamondlike carbon, will undoubtedly take place in the future. Although high-pressure synthetic diamond and natural diamond are used in the industrial market, their use in tribological applications has been limited because of their small size and high cost and their need to be bonded to a substrate in a separate operation.

Low-pressure diamond synthesis was discovered in the 1970's [8.3, 8.4]. In the 1980's synthetic diamond was produced in coating form by using a variety of low-pressure, vapor-phase synthesis techniques under relatively benign conditions. The low-pressure, vapor-phase process is based on chemical vapor deposition (CVD), a relatively inexpensive process similar to carbide and nitride processing. The material produced is often called CVD diamond, vapor-phase diamond, or diamond coating. CVD diamond coatings 1 mm or more thick are now routinely produced. After removing the substrate a free-standing shape of CVD diamond coating, normally polycrystalline, remains with good integrity and properties similar to those of single-crystal natural and high-pressure synthetic diamond.

Another new form of carbon coating was developed in the 1980's and is now available. A metastable carbon produced as a thin coating by low-pressure synthesis, it is known as diamondlike carbon (DLC). Although DLC has properties similar to those of CVD diamond, it cannot be obtained as thick monolithic shapes, at least with the present technology. A revolution in diamond technology and the diamond business is in progress as the low-pressure process becomes an industrial reality. It will soon be possible to take advantage of the outstanding properties of diamond to develop a myriad of new applications. The production of large diamond films or sheets at low cost is a distinct possibility in the not-too-distant future and may lead to drastic changes in the existing technological and business structure.

In the field of tribology synthetic diamond film technology looks promising and could edge into tribological and tooling applications. However, coating specialists and researchers still tackle such problems as enhancing adhesion to substrates (including steel), increasing bending strength, lowering deposition temperature, speeding up deposition (production) rates, and lowering costs. CVD diamond and DLC coatings offer a broader potential in the field of tribology than do natural and high-pressure synthetic diamond because size and eventually cost will be less of a limitation. For example, CVD diamond has been deposited on a 20-cm-diameter area, and DLC has been deposited on a 200-cm knife-edge. For large areas ($>5 \text{ mm}^2$) CVD diamond and DLC are the only forms of diamond or diamondlike materials that seem economically viable. These films open the door to tribological technology and design engineering that can take full advantage of diamond's intrinsic properties to make solid-lubricating, wear-resistant, erosion- and corrosion-resistant, and protective coatings. These CVD diamond and DLC materials could offer lively new solutions to important engineering problems and exciting challenges to the tribologist or designer who seeks to cost-effectively exploit their potential. The develop-

ment of safe and economic applications for diamond materials in competition with conventional tribological materials requires understanding their behavior and taking innovative approaches to manufacturing.

This chapter reviews the structures and properties of natural and synthetic diamond to gain a better understanding of the tribological behavior of these materials and related materials to be described in the following chapters.

8.2 Atomic and Crystal Structure of Diamond

Understanding diamond's behavior and properties requires a clear picture of the atomic configuration of the carbon atom and the various ways in which it bonds to other carbon atoms [8.1–8.8].

8.2.1 Tetragonal sp^3 Orbital and Trigonal sp^2 Orbital of Carbon Hybrid

The six electrons of the carbon atom in the ground state (i.e., a single atom) are configured as $1s^2 2s^2 2p^2$ (i.e., two electrons are in the K shell (1s) and four are in the L shell, two in the 2s orbital and two in the 2p orbital). The $1s^2 2s^2 2p^2$ configuration of the carbon atom does not account for the tetrahedral symmetry found in structures such as diamond or methane (CH_4). The carbon atom is bonded to four other carbon atoms in the case of diamond, or to four atoms of hydrogen in the case of methane. In both cases the four bonds are of equal strength.

To have an electron configuration that would account for this tetrahedral symmetry, the structure of the carbon atom must be altered to a state with four valence electrons instead of two, each in a separate orbital and each with its spin uncoupled from the other electrons. This alteration occurs when hybrid atomic orbitals form in which the electrons in the L shell of the ground-state atom are rearranged, one 2s electron being promoted (or lifted) to the higher orbital 2p. The new orbitals are called hybrids, since they combine the 2s and 2p orbitals. They are labeled sp^3 , since they are formed from one s orbital and three p orbitals.

The hybridization accounts for the tetrahedral symmetry and the valence state of 4, with four $2sp^3$ orbitals in the diamond atomic structure. The orbitals are bonded to the orbitals of four other carbon atoms with a strong covalent bond (i.e., the atoms share a pair of electrons) to form a regular tetrahedron with equal angles to each other of $109^\circ 28'$, as shown in Fig. 8.1(a).

In addition to the sp^3 -tetragonal hybrid orbital, two other orbitals complete the series of electronic building blocks of all carbon allotropes and compounds: the sp^2 and sp orbitals. Whereas the sp^3 orbital is the key to diamond and aliphatic compounds, the sp^2 (or trigonal) orbital is the basis of all graphitic structures and aromatic compounds: graphite, graphitic materials, amorphous carbon, and other carbon materials.

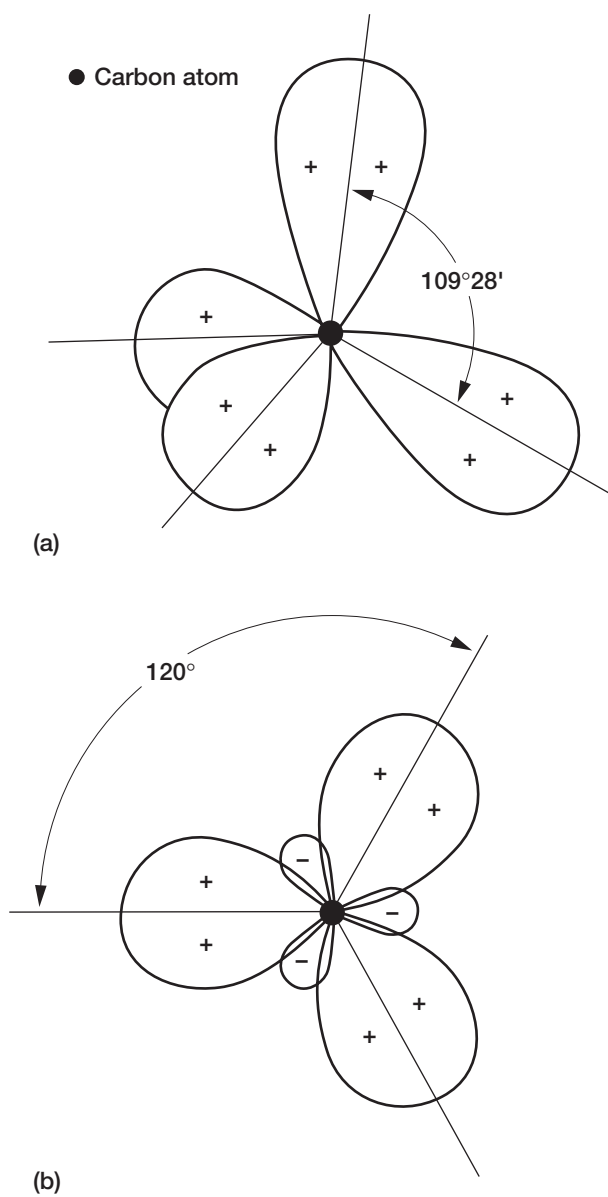


Figure 8.1.— sp^3 and sp^2 hybridization of carbon orbitals.
 (a) Four sp^3 orbitals of carbon atom. (Negative lobes omitted for clarity.) (b) Planar section of sp^2 hybrid orbitals of carbon atom.

The mechanism of the sp^2 hybridization is somewhat different from that of the sp^3 hybridization. The electrons in the L shell of the ground-state atom are rearranged, one 2s electron being promoted and combined with two of the 2p orbitals (hence, the designation sp^2) to form three sp^2 orbitals and an unhybridized free (or delocalized) p orbital electron. The valence state is now 4.

The calculated electron-density contour of the sp^2 orbitals is similar in shape to that of the sp^3 orbitals. Like the sp^3 orbital the sp^2 is directional and is called a sigma (σ) orbital; and the bond, a sigma bond. These three identical sp^2 orbitals are in the same plane, and their orientation of maximum probability forms equal angles to each other of 120° as shown in Fig. 8.1(b).

The fourth orbital (i.e., the delocalized, nonhybridized p electron) is directed perpendicular to the plane of the three sp^2 orbitals and becomes available to form the subsidiary pi (π) bond with other atoms.

8.2.2 Carbon Covalent sp^3 and sp^2 Bonds

In diamond each tetrahedron of the hybridized carbon atom combines with four other hybridized atoms (tetrahedra) to form a strongly bonded, three-dimensional, entirely covalent lattice structure, as shown schematically in Fig. 8.2. The covalent link between the carbon atoms of diamond is characterized by a short bond length (0.154 nm) and a high bond energy (711 kJ/mol).

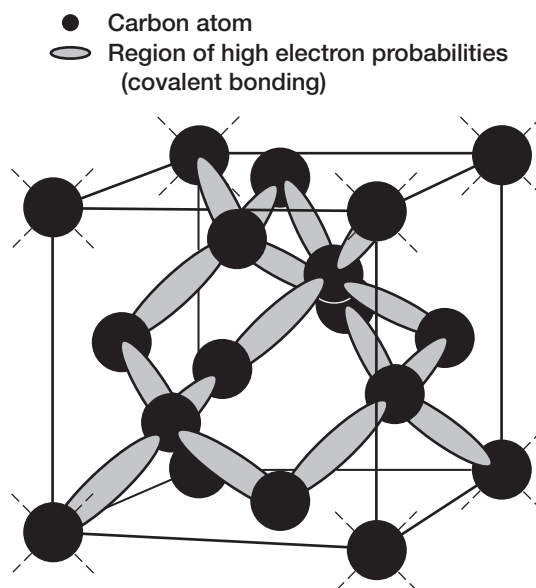


Figure 8.2.—Three-dimensional representation of sp^3 covalent bonding (lattice structure).

Diamond has two crystalline structures, one with cubic symmetry (by far the more common and stable) and one with hexagonal symmetry (found in nature as the mineral lonsdaleite). Cubic diamond will be referred to simply as “diamond” in this book. Table 8.1 summarizes the structure and properties important to tribologists and lubrication engineers. For comparison the table includes the structure and properties of graphite.

The cubic structure of diamond can be visualized as a stacking of puckered infinite layers (the $\{111\}$ planes), as shown in Fig. 8.3(a). The stacking sequence of the $\{111\}$ planes is ABCABC, so that every third layer is identical.

Graphite is composed of a series of stacked parallel layers (Fig. 8.3(b)) with trigonal sp^2 bonding. Within each layer the carbon atom is bonded to three others, forming a series of continuous hexagons in what can be considered as an essentially infinite two-dimensional molecule. Each sp^2 -hybridized carbon atom combines with three other sp^2 -hybridized atoms to form a series of hexagonal structures, all located in parallel flat layers (Fig. 8.3(b)). Like the sp^3 bond the sp^2 bond is covalent. It is also short (0.1415 nm) and strong (524 kJ/mol) because of the three sp^2 valence electrons and the small size of the atom. The fourth valency (i.e., the free delocalized electron) is oriented perpendicular to this plane. The hybridized fourth valence electron is paired with another delocalized electron from the adjacent layer by a much weaker van der Waals bond (a secondary bond arising from structural polarization) of only 7 kJ/mol (π bond). Thus, graphite’s physical properties have marked layerlike anisotropy.

The most common stacking sequence of the graphite crystal is hexagonal (alpha) with a –ABABAB– stacking order (i.e., the carbon atoms in alternate layers are superimposed over each other, Fig. 8.3(b)). Carbon is the only element to have this particular layered hexagonal structure. The crystal lattice parameters (i.e., the relative positions of its carbon atoms) are $a_0 = 0.246$ nm and $c_0 = 0.6708$ nm. Hexagonal graphite is the thermodynamically stable form of graphite.

TABLE 8.1.—CRYSTAL STRUCTURE OF DIAMOND AND GRAPHITE

Structure	Diamond	Graphite
Carbon bonding (bond energy, kJ/mol)	Covalent sp^3 (711)	Covalent sp^2 (524); van der Waals (7)
Crystalline form	Cubic; hexagonal	Hexagonal; rhombohedral
Crystal lattice parameter, nm	Cubic, 0.3567	Hexagonal: $a_0 = 0.246$ $c_0 = 0.6708$
Common crystal face	$\{111\}$, $\{011\}$, $\{001\}$	$\{0001\}$, $\{10\bar{1}0\}$, $\{10\bar{1}1\}$, $\{\bar{1}012\}$
Cleavage and slip plane	$\{111\}$	$\{0001\}$

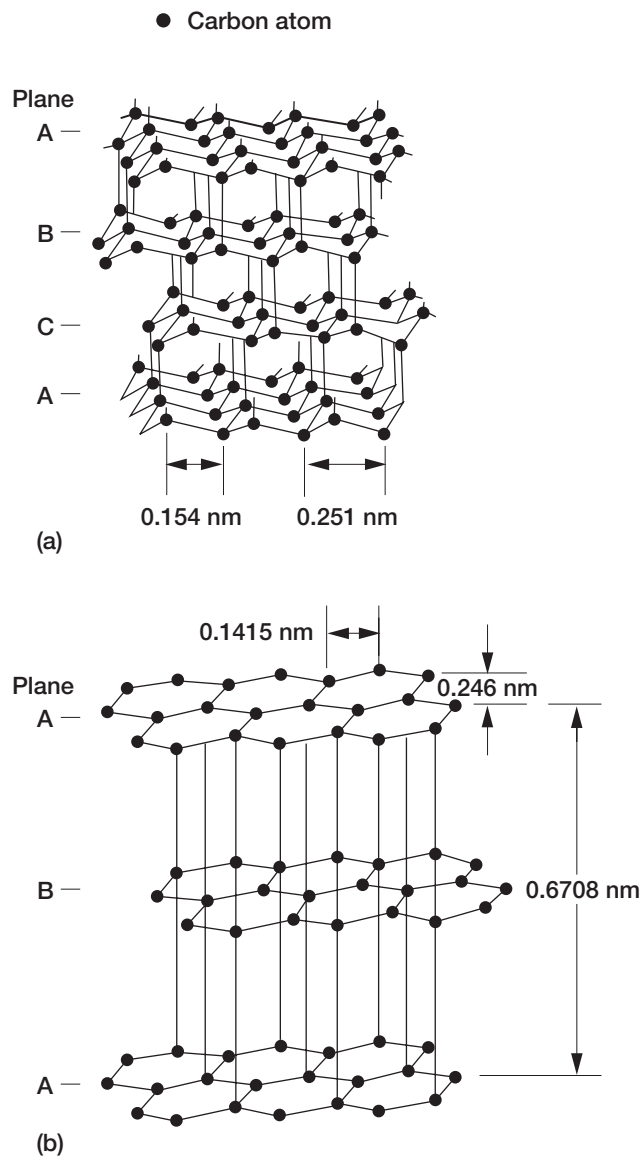


Figure 8.3.—Schematic diagrams of crystal structures of diamond and graphite. (a) Cubic structure of diamond (ABC sequence). (b) Hexagonal structure of graphite (ABAB sequence).

8.3 Impurities

One universally accepted classification of diamond is based on the nature and amount of impurities contained within the structure (Table 8.2). Diamond, synthetic or natural, is never completely free of impurities. These impurities are divided into two principal types: (1) lattice impurities (type I), which consist of foreign elements incorporated into the crystalline lattice, the foreign atom replacing a carbon atom; (2) inclusions (type II), separate particles that are not part of the lattice and usually consist of aluminum, magnesium, or calcium, such as olivine and garnet. Only nitrogen and boron are known with certainty to be incorporated into the diamond lattice. These two elements have small atomic radii and fit readily within the diamond structure. Nitrogen is present in all natural diamond, with up to 2000 ppm in type Ia diamond. Boron is present in natural type IIb diamond (up to 100 ppm) and in specifically doped type IIb synthetic diamond (270 ppm). Many other impurities have been detected but are believed to be inclusions. For example, up to 10 ppm of aluminum is frequently found in natural diamond, and synthetic diamond may contain nickel or iron inclusions that occupy as much as 10% of the crystals. The properties of diamond are susceptible to these impurities, and even a minute amount of a foreign element such as nitrogen can cause drastic changes. These effects are shown in Table 8.2 and discussed in Section 8.4.

The tetrahedral bonding configuration (Fig. 8.2) and the strong carbon-carbon bond give diamond its unique properties (summarized in Table 8.3). For comparison the table also includes the properties of graphite. Determining the properties of diamond is difficult, and published data are still limited. Small specimen size, imperfections, and impurities contribute to the considerable spread in reported values often found in the literature.

TABLE 8.2.—CLASSIFICATION AND CHARACTERISTICS OF DIAMOND

Lattice impurity type	Thermal conductivity, W/m-°C	Electric resistivity, ohm-cm	Color	Impurity		Synthetic diamond	Abundance in natural diamond, percent
				Nitrogen, ppm	Others, ppm		
Ia	800	^a 10 ⁴ –10 ¹⁶	Clear to yellow	^b ≈2000	-----	None	≈98
Ib	800–1700	^a 10 ⁴ –10 ¹⁶	Green to brown	^c 10 ² –10 ³	^d 10 ⁴ –10 ⁵	Powder	≈0.1
Ib	2000	^a 10 ¹⁶	Yellow	^c 1–100	-----	Single crystal	≈0.1
IIa	2000	^a 10 ¹⁶	Colorless, clear	^e ≈1	-----	Single crystal	1–2
IIb	-----	^f 10–10 ⁴	Blue	≈1	^g ≈100	Single crystal	≈0

^aInsulator.

^bPlatelet form.

^cDispersed in lattice.

^dSolvent metals.

^eHigh purity.

^fSemiconductor P type.

^gBoron.

TABLE 8.3.—PROPERTIES OF DIAMOND AND GRAPHITE

Property	Diamond	Graphite
Density, g/cm ³	3.52	2.26
Young's modulus, GPa	^a 910–1250	Single crystal: 1060 (a direction) 36.5 (c direction) Pyrolytic graphite, 28–31 Molded graphite, 5–10
Poisson's ratio	^b 0.10–0.29	-----
Compression strength, GPa	8.68–16.53	0.065–0.089
Vickers hardness, GPa	60–100	Pyrolytic graphite, 2.4–3.6 Molded graphite, 3.9–9.8
Thermal conductivity at 25 °C, W/m-°C	600–1000 (type Ia) 2000–2100 (type II)	Pyrolytic graphite: a and b directions, 190–390 c direction, 1–3 Molded graphite, 31–159
Coefficient of thermal expansion at 25 to 200 °C, 10 ⁻⁶ /deg C	^c 0.8–4.8	Pyrolytic graphite: a and b directions, –1 to 1 c direction, 15–25 Molded graphite, 3.2–5.7
Specific heat at 25 °C, kJ/kg-K	0.502–0.519	0.690–0.719

^aTypical values, 1050 and 1054.^bTypical value, 0.2.^c1.5 to 4.8 at 127 to 927 °C.

8.4 Mechanical Properties of Diamond

The properties described here are those of both natural and synthetic diamond. See the reference list [8.9–8.25] for further reading.

8.4.1 Strength and Hertzian Fracture Properties

Materials with high hardness are usually brittle and diamond is no exception. Diamond behaves as a brittle solid and fractures along its cleavage planes. The fracture behavior of diamond is dominated by cleavage on the {111} plane, but cleavage fracture has also been observed along the other planes, such as {211}, {110}, and {322}, since the theoretical cleavage energy differences between planes are small, as shown in Table 8.4. The cleavage energies are consistent with the order of the cleavage planes, from easiest to hardest to cleave.

Knowledge of the fracture stress and crack patterns produced in diamond is important in understanding tribological phenomena, such as wear, erosion, and abrasion. Such knowledge can be gained from crack patterns produced in natural and synthetic diamond by spherical indenters under normal loading. An indenter loaded onto the surface of a specimen generally produces a local damage zone comparable to the dimensions of the contact area (Fig. 8.4(a)). These results have interest for two reasons. First, it is important to know diamond's fracture behavior, particularly the crack patterns and fracture stress under conditions arising in its tribological applications. Second, indentation techniques are the main method for measuring the strength of materials.

TABLE 8.4.—THEORETICAL CLEAVAGE
ENERGIES FOR DIAMOND

Plane	Angle between plane and {111} plane	Cleavage energy, ^a J/m ²
111	0°, 70°32'	10.6
332	10°0'	11.7
221	15°48'	12.2
331	22°0'	12.6
110	35°16', 90°	13.0
322	11°24'	13.4
321	22°12'	14.3
211	19°28'	15.0
320	36°48'	15.3
210	39°14'	16.4
311	29°30'	16.6
100	54°44'	18.4

^aTo obtain fracture surface energy, divide by 2.

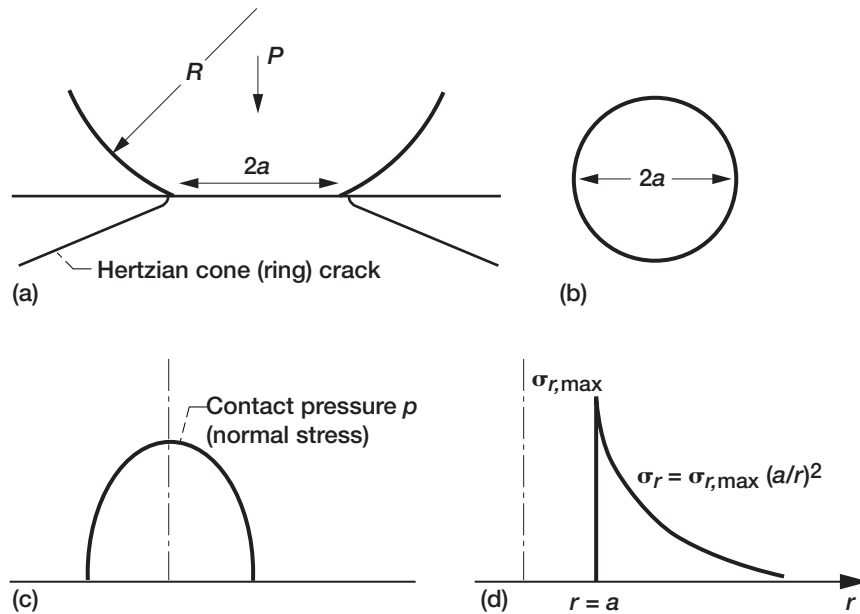


Figure 8.4.—Geometry of Hertzian cone (ring) crack and stress distributions formed by sphere loaded normally onto plane surface of brittle material.

(a) Hertzian ring crack. (b) Contact area (radius of contact circle a).

(c) Distribution of normal stress p . (d) Distribution of tensile stress σ_r .

The basis for treating the contact problem is the elasticity analysis of Hertz [8.9]. In the Hertzian method of measuring fracture stress a hard, spherical indenter is pressed against the solid under normal loading P , and the load at fracture is measured. The radius of the contact circle a (Fig. 8.4(b)) is given by

$$a^3 = \frac{3}{4} PR \left(\frac{1 - \nu_1^2}{E_1} + \frac{1 - \nu_2^2}{E_2} \right) \quad (8.1)$$

where R is the radius of the spherical indenter and E_1 , ν_1 and E_2 , ν_2 are the Young's modulus and Poisson's ratio of the solid and the indenter, respectively. The radius of the contact circle is proportional to $P^{1/3}$. And then the area of contact πa^2 is proportional to $P^{2/3}$. The mean pressure (normal stress) over the contact area $p_{\text{mean}} = P/\pi a^2$ varies as $P^{1/3}$. This normal stress is not uniform over the circular area of contact but is highest at the center and falls to zero at the edge. Figure 8.4(c) shows the distribution of normal stress; the maximum normal stress, at the center of the contact circle, is 3/2 times the mean normal stress. Within the contact circle the stress field becomes largely compressive, but outside the contact circle there is a tensile stress field in the surface.

The tensile stress σ_r in the plane surface has a maximum value $\sigma_{r,\text{max}}$ at the edge of the contact area ($r = a$), given by

$$\sigma_{r,\text{max}} = (1 - 2\nu_1) p_{\text{mean}}/2 \quad (8.2)$$

$$p_{\text{mean}} = P/\pi a^2 \quad (8.3)$$

The maximum tensile stress $\sigma_{r,\text{max}}$ acts radially and parallel to the surface and gives rise to fracture.

This tensile stress falls off with increasing radial distance (Fig. 8.4(d)) according to

$$\sigma_r = \frac{(1 - 2\nu_1)P}{2\pi r^2} \quad (8.4)$$

$$\sigma_r = \sigma_{r,\text{max}} (a/r)^2 \quad (8.5)$$

r being the radial distance from the center of the contact. Below the surface and outside the contact area the component of tensile stress diminishes rapidly with depth and distance. A tensile "skin" layer consequently exists beyond the immediate indentation site, thereby affording highly favorable conditions for crack initiation. At some critical loading the elastic limit of the specimen will be exceeded, and

irreversible deformation will occur. In a brittle specimen the critical event is marked by the sudden development of the so-called Hertzian cone (ring) crack (Fig. 8.4(a)).

With a brittle solid, such as glass, a ring crack forms in the tensile region. Such ring cracks have also been found and studied on diamond surfaces. When ring cracks develop in brittle materials, they usually start a little beyond the edge of the contact circle (i.e., not at the point predicted by the Hertzian analysis to have the maximum tensile stress). Several workers have tried to explain this result in terms of a size distribution of defects in the solid surface.

Another important factor is the interfacial shear stresses that arise when the indenter and indented materials have different elastic properties. In this situation when the solids are pressed into contact, the materials on either side of the contact interface will want to move by unequal amounts. Relative movement at the interface will be affected by frictional forces. Clearly, the Hertzian stress field, which neglects such interfacial effects, will be modified. If the indenter is the more rigid material, the interfacial stresses reduce the movement of the indented solid surface. The modified peak radial tensile stress is now less than that given by Eq. (8.4) and exists slightly farther out. In other words, the material fails at an artificially high fracture load and should do so at $r > a$. When the indenter is the more compliant material, the effect is to intensify the radial stresses, resulting in an artificially low fracture load. If this interfacial effect is small, it can be neglected.

Comparison of diamond with sapphire (alumina) and silicon.—Cleavage cracks emerging on a crystalline surface form inherent patterns on the surface. Figure 8.5, for example, shows well-developed ring cracks produced on silicon {100}, sapphire {0001}, and natural diamond {111} during experiments in which the specimens were indented with 200- μm - or 500- μm -radius spherical diamond indenters [8.22]. Cleavage occurred mostly along the {111} planes in both silicon and diamond and along the $\{\bar{1}012\}$ planes in sapphire. In silicon the ring cracks (following the {111} cleavage planes) on the {100} plane formed a square pattern in the $\langle 110 \rangle$ direction. In sapphire the ring cracks (following the $\{\bar{1}012\}$ cleavage planes) on the {0001} plane formed a triangular or hexagonal pattern. In diamond the ring cracks (following the {111} cleavage planes) on the {111} plane formed a triangular or hexagonal pattern in the $\langle 110 \rangle$ direction.

Figure 8.6 presents the maximum tensile stress $\sigma_{r,\text{max}}$, or the tensile strength, which acts normal to cleavage planes at the edge of the Hertzian contact circle and gives rise to fracture on silicon {100}, sapphire {0001}, natural diamond {111}, and synthetic diamond {111} as a function of indenter radius. Indenter radius had a marked effect on Hertzian fracture and on the maximum tensile stress to fracture. The greater the indenter radius, the lower the maximum tensile stress to fracture. Further, the values of maximum tensile stress (tensile strength) shown in Fig. 8.6 are of the same order as the theoretical strengths for the corresponding materials. The theoretical strengths are approximately 1/10th of the Young's moduli, which are 167 GPa for silicon, 380 GPa for sapphire, and 1020 GPa for natural and synthetic diamond. The tensile strengths of the materials investigated herein were, in ascending order, silicon, sapphire, natural diamond, and synthetic diamond.

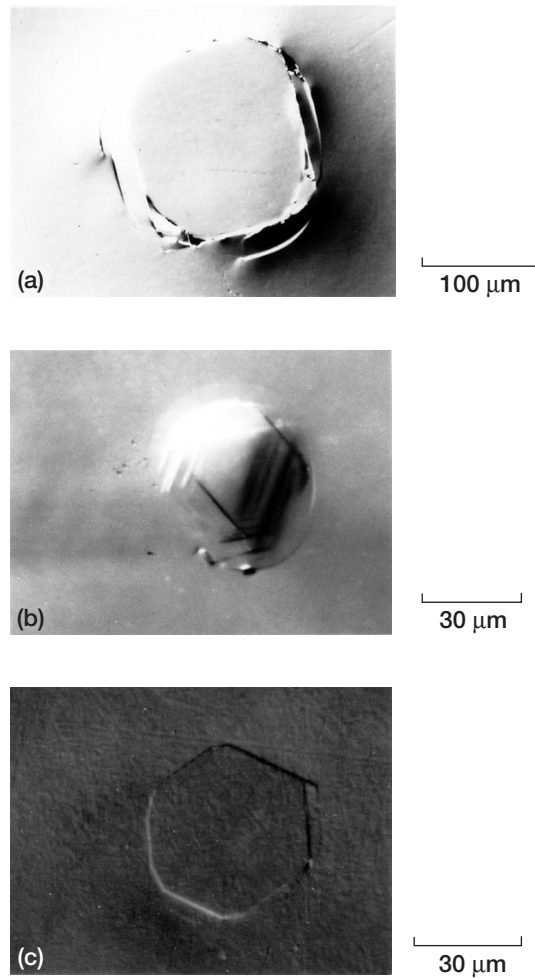


Figure 8.5.—Typical ring cracks in various specimens. (a) Silicon {100}. Indenter radius, 500 μm. (b) Sapphire {0001}. Indenter radius, 200 μm. (c) Natural diamond {111}. Indenter radius, 200 μm.

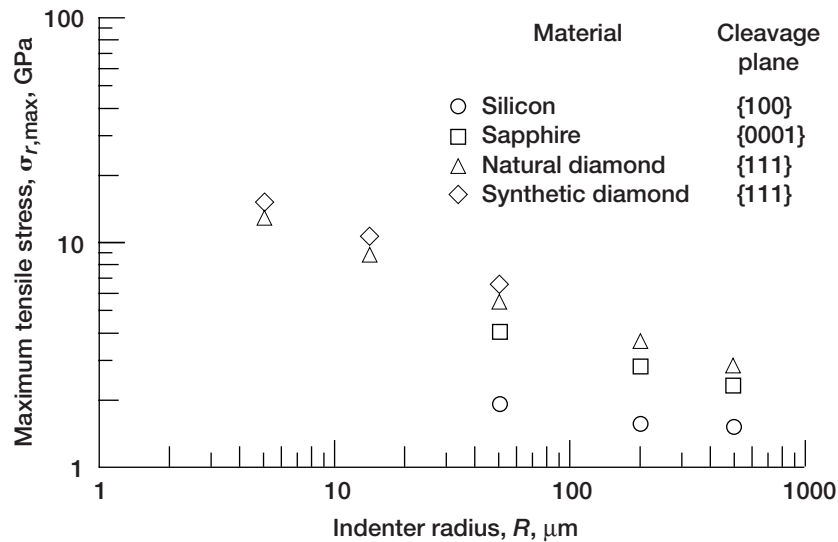


Figure 8.6.—Maximum tensile stress normal to cleavage plane at edge of contact circle for silicon, sapphire, and natural and synthetic diamond as function of indenter radius.

Anisotropy in tensile strength.—Figure 8.7 presents ring cracks formed on polished {111}, {100}, and {110} surfaces of cutting-tool-grade natural diamond by spherical diamond indenters [8.21]. All cleavage fractures occurred along the {111} planes in diamond. On the {111} and {110} diamond surfaces ring cracks formed a triangular or hexagonal pattern in the $\langle 110 \rangle$ direction. On the {100} diamond surface ring cracks formed a square pattern in the $\langle 110 \rangle$ direction. As shown in Fig. 8.8 the anisotropy in the mean maximum tensile stress to fracture on the {111}, {100}, and {110} diamond surfaces is small, but the critical load to fracture greatly varies with the surfaces [8.21].

Effect of impurities on tensile strength.—As shown (especially in Fig. 8.8) determining diamond's properties is difficult, and there is considerable spread in the values reported in the literature. Impurities, particularly nitrogen, considerably alter the tensile strength, as shown in Fig. 8.9. When the {100} surfaces of single-crystal synthetic diamond containing 1 ppm to nearly 300 ppm of nitrogen were indented with a 5- μm -radius spherical diamond indenter, nitrogen altered the maximum tensile stress to fracture (tensile strength). The tensile strength decreased with an increase in nitrogen concentration. In other work, when the {100} surfaces of natural diamond containing approximately 2000 ppm of nitrogen were indented with a 5- μm -radius spherical diamond indenter, the tensile strength consistently decreased with an increase in nitrogen concentration and ranged from 15 to 25 GPa.

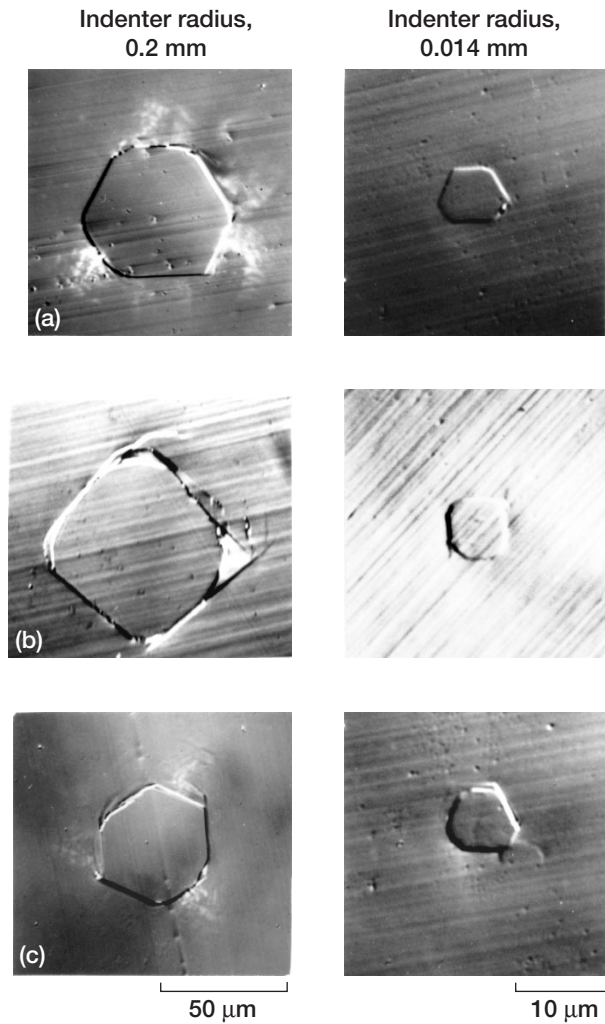


Figure 8.7.—Ring cracks on various polished surfaces of cutting-tool-grade natural diamond. (a) {111}. (b) {100}. (c) {110}.

8.4.2 Indentation Hardness

As described in the previous section, spherical indenters develop tensile stresses around the contact area that encourage brittle fracture rather than plastic flow. Pyramidal indenters (used by Knoop, Vickers, and Berkovich), however, produce rhombohedral, square, and triangular indentations, respectively, which are plastically deformed.

The property measured by an indentation hardness test is the plastic strength of the material (i.e., the amount of plastic deformation produced). All pyramidal indenters have a further advantage in that they yield values, in terms of units of pressure, that can be compared directly with other mechanical properties, such as yield stress, yield strength, and Young's modulus.

Comparison of diamond with other solids.—It has already been established that the hardness measured for crystalline solids is very much dependent on indenter shape, normal load, temperature, crystallographic orientation of the indenter with respect to the indented plane, and impurities. The diamond crystal is the hardest known material, although theoretical works suggest that the hypothetical compound $\beta\text{-C}_3\text{N}_4$ should be as hard or even harder than diamond. This fact makes it difficult to measure diamond's hardness, since only another diamond can be used as an indenter, and may help to explain the wide variations in reported values of diamond hardness. For example, although the Knoop indenter gave a hardness range of 73.5 to 88.2 GPa for diamond {111} and the Berkovich indenter a hardness range of 17.6 to 20.1 GPa for sapphire {0001}, only the median values are shown in Fig. 8.10 [8.24]. For a given crystal the Knoop hardness values are generally lowest, and the Vickers and Berkovich indenters give similar results.

Anisotropy in indentation hardness.—The indentation hardness, like the tensile strength, is intrinsically anisotropic. Figure 8.11 presents the anisotropic phenomenon in the two major types of diamond indented at room temperature with a 9.8-N load on mechanically polished surfaces. The results clearly show the type II diamonds to be significantly harder than the type I. The anisotropy in the hardness of crystals is controlled by their crystallographic structures and the relevant operative slip systems. The observed anisotropy of diamond was predicted and explained by models based on resolved shear stresses developed on the primary {111} $\langle 110 \rangle$ slip systems in the bulk of the crystal beneath the indenter. The easiest plane to indent by a Knoop indenter is the {111} in the $\langle 110 \rangle$ direction. Contrary to indentation measurements the {111} planes are generally the most difficult to abrade.

Effect of impurities on indentation hardness.—Impurities, particularly nitrogen, considerably alter the indentation hardness. Polished {100} surfaces of single-crystal synthetic diamond (type Ib) containing 1 ppm to nearly 100 ppm of nitrogen and natural diamond (type Ia) containing up to 2000 ppm of nitrogen were indented with a Knoop diamond indenter. As shown in Fig. 8.12 type Ia natural diamond invariably contained more nitrogen impurities (e.g., nitrogen platelets) and thus had greater ranges of hardness values.

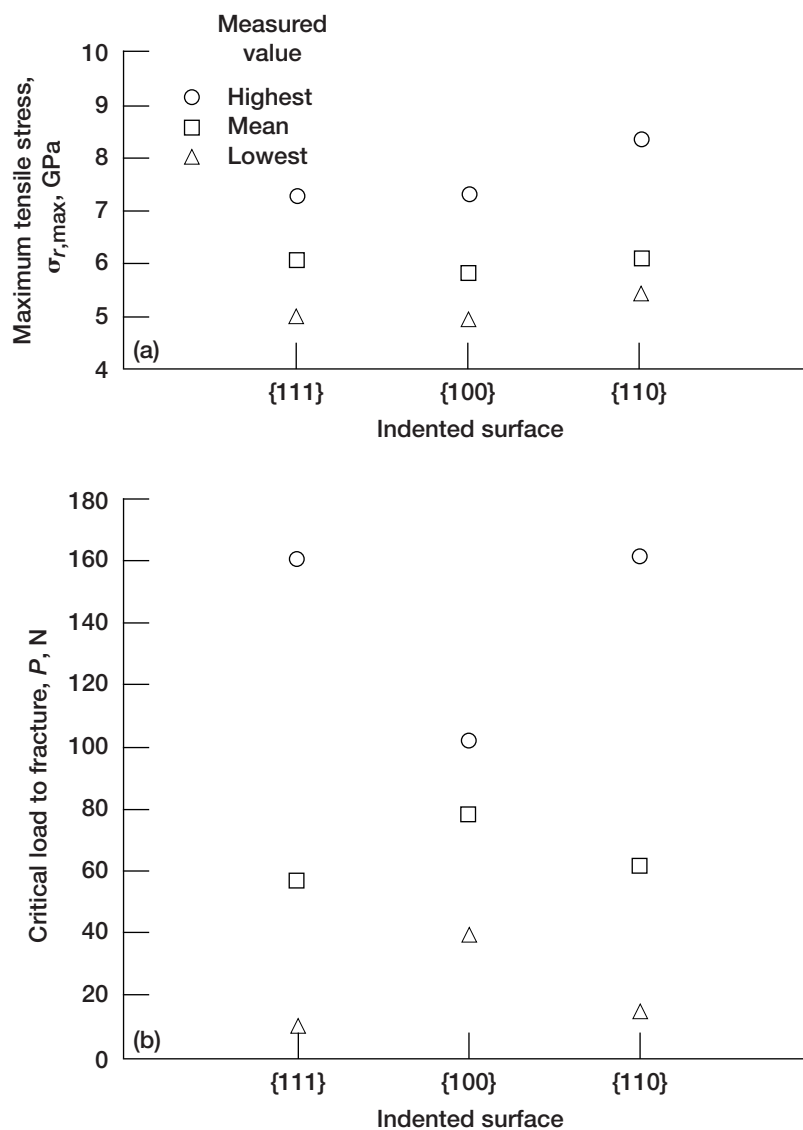


Figure 8.8.—(a) Maximum tensile stress (strength) normal to cleavage plane at edge of contact circle for and (b) critical load to fracture on {111}, {100}, and {110} surfaces of cutting-tool-grade natural diamond.

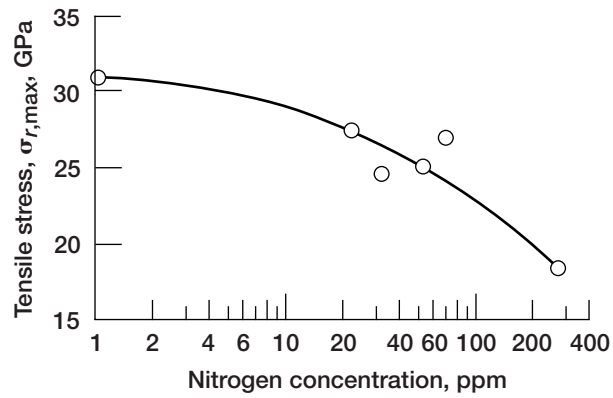


Figure 8.9.—Maximum tensile stress (strength) of synthetic diamond in Hertzian contact with 5-mm-radius diamond indenter as function of nitrogen concentration.

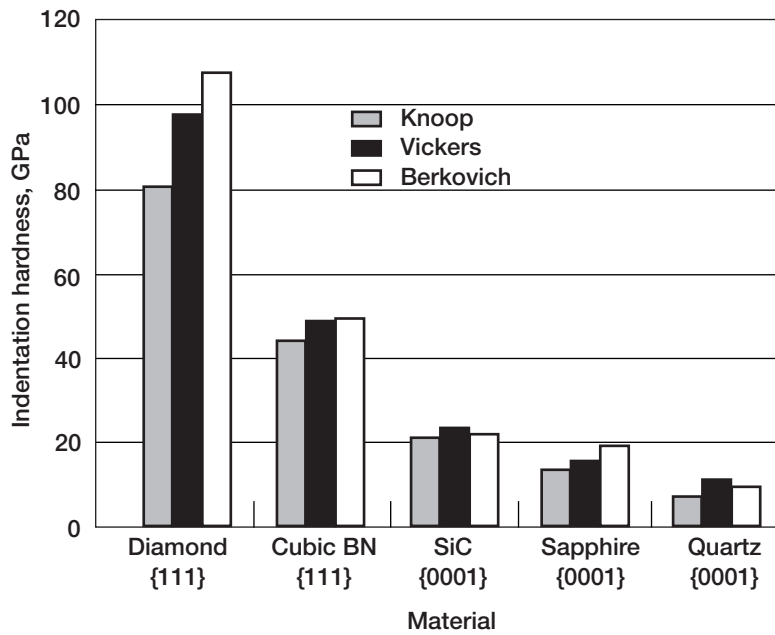


Figure 8.10.—Indentation hardnesses for diamond and other solid materials.

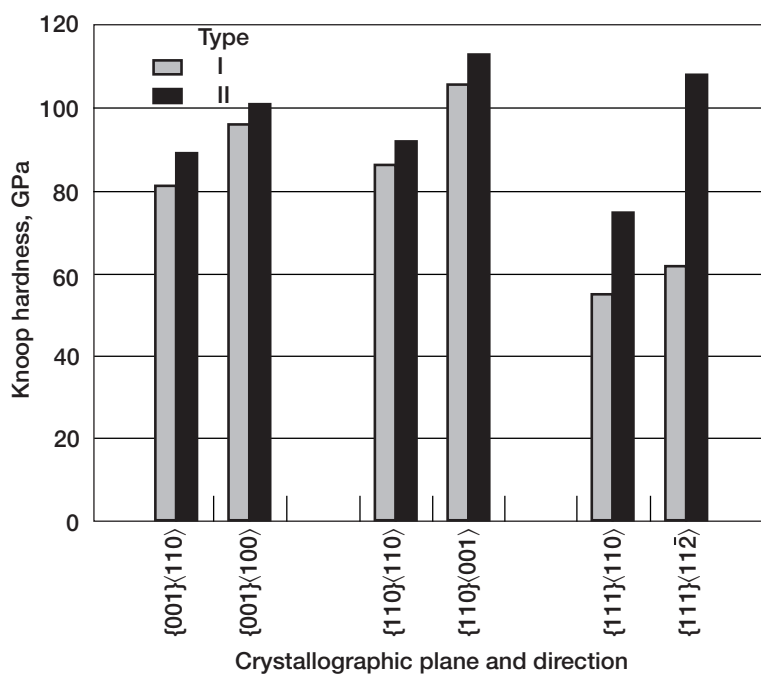


Figure 8.11.—Anisotropic Knoop hardness for two types of diamond.

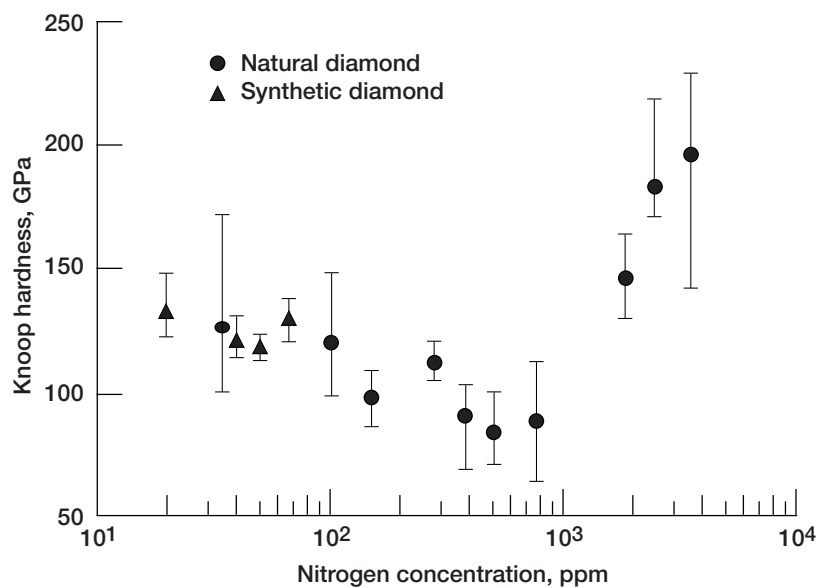


Figure 8.12.—Knoop hardness of synthetic and natural diamond as function of nitrogen concentration.

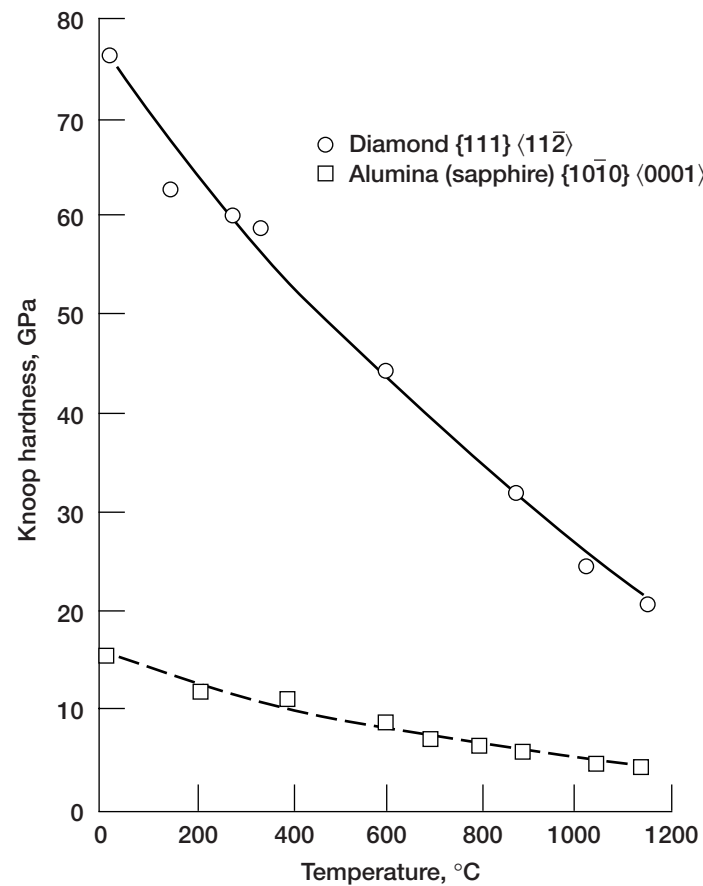


Figure 8.13.—Knoop hardness of diamond {111} and sapphire (alumina) {10 $\bar{1}$ 0} surfaces as function of temperature.

Effect of temperature on indentation hardness.—Hardness values for single-crystal diamond and alumina were obtained by using a Knoop indenter oriented in $\langle 11\bar{2} \rangle$ on {111} and $\langle 0001 \rangle$ on {10 $\bar{1}$ 0}, respectively. The results (Fig. 8.13) confirm that, although its hardness decreased with increasing temperature and there was a corresponding increase in plastic deformation, at 1200 °C diamond was still harder than alumina at room temperature. Also, because diamond has the highest thermal conductivity of any material at room temperature, cracking due to thermal shock is not likely to be a problem, in contrast to alumina.

References

- 8.1 H.O. Pierson, *Handbook of Carbon, Graphite, Diamond and Fullerenes: Properties, Processing, and Applications*, Noyes Publications, Park Ridge, NJ, 1993.
- 8.2 J.E. Field (ed.), *The Properties of Diamond*, Academic Press, New York, 1979.
- 8.3 R.E. Clausing, et al. (eds.), *Diamond and Diamondlike Films and Coatings*, Plenum Press, New York, 1991.
- 8.4 P.D. Gigl, New synthesis techniques: properties and applications for industrial diamond, Presented at the IDA Ultrahard Materials Seminar, Toronto, Ontario, Canada, 1989.
- 8.5 P.G. Lurie and J.M. Wilson, The diamond surface, *Surf. Sci.* 65: 476–498 (1977).
- 8.6 J. Wei and J.T. Yates, Jr., Diamond surface chemistry: I—A review, *Crit. Rev. Surf. Chem.* 5: 1–71 (1995).
- 8.7 A.G. Guy, *Elements of Physical Metallurgy*, Addison-Wesley Publishing Co., Reading, MA, 1959.
- 8.8 J.P. Hirth and J. Lothe, *Theory of Dislocations*, McGraw-Hill, New York, 1968, pp. 353–363.
- 8.9 H. Hertz, Über die Berührung fester elastischer Körper, *J. Reine und Angew. Math.* 92: 156–171 (1881).
- 8.10 S. Timoshenko and J.N. Goodier, *Theory of Elasticity*, McGraw-Hill, New York, 1951, p. 372.
- 8.11 F.C. Frank and B.R. Lawn, On the theory of Hertzian fracture, *Proc. R. Soc. (London), Ser. A* 299: 291–306 (1967).
- 8.12 B.R. Lawn, Hertzian fracture in single crystals with the diamond structure, *J. Appl. Phys.* 39, 10: 4828–4836 (1968).
- 8.13 B.R. Lawn and M.V. Swain, Microfracture beneath point indentations in brittle solids, *J. Mater. Sci.* 10: 113–122 (1975).
- 8.14 B.R. Lawn and T.R. Wilshaw, *Fracture of Brittle Solids*, Cambridge University Press, 1975.
- 8.15 S. Tolansky and V.R. Howes, Induction of ring cracks on diamond surfaces, *Proc. Phys. Soc. (London), Sect. B* 70: 521–526 (1957).
- 8.16 M. Seal, The abrasion of diamond, *Proc. R. Soc. (London), Ser. A* 248: 379–393 (1958).
- 8.17 V.R. Howes, The critical stress for the production of pressure crack figures on diamond faces, *Proc. Phys. Soc.* 74: 48–52 (1959).
- 8.18 C.A. Brookes, Indentation hardness of diamond, *Diamond Research*, 1971, pp. 12–15.
- 8.19 W.R. Tyson, Theoretical strength of perfect crystals, *Phil. Mag.* 14: 925–936 (1966).
- 8.20 N. Ikawa, S. Shimada, and H. Tsuwa, Microfracture of diamond as fine tool material, *CIRP Ann.* 31, 1: 71–74 (1982).
- 8.21 N. Ikawa, S. Shimada, and T. Ono, Microstrength of diamond, *Technology Reports of Osaka University* 26, 1298: 245–254 (1976).
- 8.22 N. Ikawa and S. Shimada, Microstrength measurement of brittle materials, *Technology Reports of Osaka University* 31, 1622: 315–323 (1981).
- 8.23 S. Bhagavantam and J. Bhimasenachar, Elastic constants of diamond, *Proc. R. Soc. (London), Ser. A* 187: 381–384 (1946).
- 8.24 C.A. Brooks, Plastic deformation and anisotropy in the hardness of diamond, *Nature* 228: 660–661 (1970).
- 8.25 R.M. Chrenko and H.M. Strong, Physical properties of diamond, General Electric Technical Information Series No. 75CRD089, 1975, pp. 1–45.

REPORT DOCUMENTATION PAGE			Form Approved OMB No. 0704-0188	
Public reporting burden for this collection of information is estimated to average 1 hour per response, including the time for reviewing instructions, searching existing data sources, gathering and maintaining the data needed, and completing and reviewing the collection of information. Send comments regarding this burden estimate or any other aspect of this collection of information, including suggestions for reducing this burden, to Washington Headquarters Services, Directorate for Information Operations and Reports, 1215 Jefferson Davis Highway, Suite 1204, Arlington, VA 22202-4302, and to the Office of Management and Budget, Paperwork Reduction Project (0704-0188), Washington, DC 20503.				
1. AGENCY USE ONLY (Leave blank)		2. REPORT DATE June 1998		3. REPORT TYPE AND DATES COVERED Technical Memorandum
4. TITLE AND SUBTITLE Structures and Mechanical Properties of Natural and Synthetic Diamonds			5. FUNDING NUMBERS WU-523-22-13-00	
6. AUTHOR(S) Kazuhisa Miyoshi				
7. PERFORMING ORGANIZATION NAME(S) AND ADDRESS(ES) National Aeronautics and Space Administration Lewis Research Center Cleveland, Ohio 44135-3191			8. PERFORMING ORGANIZATION REPORT NUMBER E-9863-8	
9. SPONSORING/MONITORING AGENCY NAME(S) AND ADDRESS(ES) National Aeronautics and Space Administration Washington, DC 20546-0001			10. SPONSORING/MONITORING AGENCY REPORT NUMBER NASA TM-1998-107249, Chapter 8	
11. SUPPLEMENTARY NOTES Responsible person, Kazuhisa Miyoshi, organization code 5140, (216) 433-6078.				
12a. DISTRIBUTION/AVAILABILITY STATEMENT Unclassified - Unlimited Subject Category: 27 This publication is available from the NASA Center for AeroSpace Information, (301) 621-0390.			12b. DISTRIBUTION CODE	
13. ABSTRACT (Maximum 200 words) A revolution in diamond technology is in progress as the low-pressure process becomes an industrial reality. It will soon be possible to take advantage of the demanding properties of diamond to develop a myriad of new applications, particularly for self-lubricating, wear, and superhard coatings. The production of large diamond films or sheets at low cost, a distinct possibility in the not-too-distant future, may drastically change tribology technology, particularly solid lubricants and lubricating materials and systems. This chapter reviews the structures and properties of natural and synthetic diamond to gain a better understanding of the tribological properties of diamond and related materials to be described in the following chapters. Atomic and crystal structure, impurities, mechanical properties, and indentation hardness of diamond are described.				
14. SUBJECT TERMS Solid lubrication; Coatings; Tribology; Fundamentals; Applications			15. NUMBER OF PAGES 27	
			16. PRICE CODE A03	
17. SECURITY CLASSIFICATION OF REPORT Unclassified	18. SECURITY CLASSIFICATION OF THIS PAGE Unclassified	19. SECURITY CLASSIFICATION OF ABSTRACT Unclassified	20. LIMITATION OF ABSTRACT	